Experimental Study of Residual Stresses in Hybrid Laser Arc and Submerged Arc-Welded 10-mm-Thick Low-Carbon Steel Plates

Andreassen, Michael Joachim; Yu, Zhenzhen; Bunn, Jeffrey R.; Nielsen, Jens Henrik

Published in:
Materials Performance and Characterization

Link to article, DOI:
10.1520/MPC20180134

Publication date:
2019

Document Version
Peer reviewed version

Experimental Study of Residual Stresses in Hybrid Laser Arc and Submerged Arc-Welded 10-mm-Thick Low-Carbon Steel Plates

Michael Joachim Andreassen[1], Zhenzhen Yu[2], Jeffrey R. Bunn[3], and Jens Henrik Nielsen[4]

ABSTRACT

Offshore structures are constantly exposed to a multi-hazard marine environment that threatens their structural integrity. This imposes a high risk for extensive structural failures while various deterioration mechanisms may degrade the available capacity of the structures. Thus, no reliable decisions can be reached regarding design, operation and survivability of the structures unless a deep comprehension of their fatigue performance is available including welding-induced residual stresses. In particular, the continuous increase in size of the weldments for the offshore wind industry needs special attention with regard to welding-induced residual stresses, as they can reduce fatigue life, promote distortion, and contribute to stress corrosion cracking. Thus, the current design methods and increased structural dimensions as well as new design and manufacturing methods need to be inspected, understood, and optimized. Related to this, there is a growing need for evaluation of the effect of welding methods with various heat input density distributions. This article deals with the influence of welding method on the welding-induced residual stresses in 10-mm-thick low-carbon structural steel plates. The residual stresses are investigated in hybrid laser-arc welded and submerged arc butt-welded steel plates

Department of Civil Engineering, Technical University of Denmark, Kgs. Lyngby, DK-2800, Denmark; 0000-0003-2565-9840
[2] *Department of Metallurgical and Materials Engineering*, *Colorado School of Mines*, Golden, CO, 80401, USA; ORCID
[3] *Oak Ridge National Laboratory*, Oak Ridge, TN, 37831, USA; 0000-0001-7738-0011
[4] Department of Civil Engineering, Technical University of Denmark, Kgs. Lyngby, DK-2800, Denmark; 0000-0003-0705-9382

by means of experimental temperature profile measurements and neutron diffraction measurements and in accordance with existing production procedures. The residual stresses were measured at three different depths in the plates. The goal of the analysis is to gain a comprehensive understanding of the distribution and development of residual stresses in relation to the welding method for better control of the residual stresses and distortion. The repeatability of the neutron diffraction measurements is also investigated and reported in this article.

Keywords

Residual Stresses, Hybrid Laser-Arc Welding, Submerged Arc Welding, Neutron Diffraction, Offshore Structures, Low Carbon Steel grade S355ML.

Introduction

Supersize monopiles used as offshore wind turbine support structures are being developed and have already been installed on several offshore wind farms. The demand for fabrication of monopiles with large wall thicknesses is high. However, the implications for design and especially the joining of cans by circumferential welding with these wall thicknesses are not yet fully understood. In particular, the welding induced residual stresses need special attention. The stresses have a negative impact on the integrity of the welded joint, as they promote distortion, reduce fatigue life, and contribute to corrosion cracking and premature failure in the welded components. Research within the field of welding residual stresses is important, as the size of structures and welds are rapidly increasing. The steel fabricators raise the demands, as deeper foundations are needed because of the design requirements.

This article deals with the influence and impact of the welding method on welding-induced residual stresses. The two welding methods investigated are submerged arc welding (SAW) and hybrid laser-arc welding (HLAW). Both welding methods are applied for a full penetration butt weld of 10-mm-thick plates. Several articles have been published on topics such as welding residual stresses, offshore structures, SAW, HLAW, and numerical welding procedures, [1, 2, 3, 4, 5].

However, publications and knowledge on the combination and interaction of these topics and parameters almost do not exist.

By investigating the welding residual stresses through experiments and in accordance with existing production procedures, an optimization of the fatigue design is expected, leading to a more efficient and improved design [6,7,8]. In this context, this research is expected to benefit the offshore industry by leading to an improved design, which consequently can be included in present norms and standards.

This article deals with a steel plate thickness of 10 mm. The experiences gained from this thickness are intended to form the basis of the techniques utilized for the study of thicker plates used for the construction of monopiles [9].

Material Tests and Results

The material used for the experiments is thermomechanically hot-rolled, low-carbon, fine-grain structural steel of grade S355ML in accordance with DS/EN 10025-7, *Hot Rolled Products of Structural Steels—Part 4: Technical Delivery Conditions for Thermomechanical Rolled Weldable Fine Grain Structural Steels* [10], which has similar chemistry and physical properties to ASTM A572/709. This steel grade is widely used for offshore structures and possesses excellent weldability. It has lower carbon content than grade S355NL steel

(normalized and rolled), which thus lowers the cold cracking tendency while increasing the toughness in the heat-affected zone. The increased performance against cold cracking makes it possible to reduce the preheating, which leads to cost reduction in terms of reduced fabrication time and energy savings. The chemical composition of the welded S355ML steel plates given by the steel manufacturer is shown in Table 1.

Table. 1: Chemical composition (in wt. pct.) of S355ML steel.

C %	Si %	Mn %	P %	S %	Al %	Cr %	Ni %	Mo %	Cu %	V %	Nb %	Ti %	N %	B %	Cae %
.082	.332	1.37	.01	.0005	.045	.024	.012	.004	.016	.003	.027	.014	.0052	.0002	.32

The material properties, such as elastic modulus, yield stress, and ultimate strength, have been determined from experiments. Thus, 25 room and high-temperature monotonic tensile tests have been performed in the temperature range of 20°C to 1000°C. The tests follow the European tensile testing standards for metallic material, [11,12]. Fig. 1 shows the tensile test setup, and Fig. 2 shows the specific tensile specimen geometry with a thickness of 10 mm.

Figure 1: High-temperature monotonic tensile test setup.

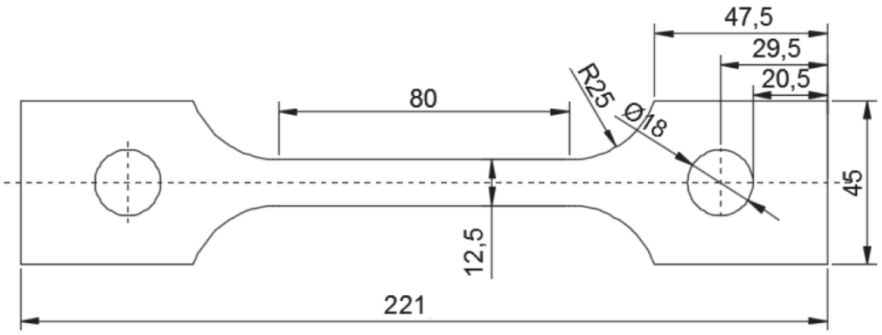

Figure 2: Tensile sample geometry in mm.

A heating furnace and MTS 312.31 250-kN universal testing machine were used. Displacement and load were logged by the testing machine, and the output was a force-displacement curve. An Instron type 2620-601 extensometer with a range of 50 mm measured the displacement over an initial gauge distance to determine the modulus of elasticity and elongation.

Table 2: Mechanical properties of S355ML steel.

Temp. (°C)	20	100	200	300	400	500	600	700	800	1000
E (MPa) x 10^5	2.18	2.03	2.15	1.86	1.06	1.54	0.91	0.53	0.39	0.14
SD (MPa) x 10^5	0.04	0.12	0.17	0.23	0.13	0.35	0.23	0.03	0.06	0.00
f_y (MPa)	404	380	366	325	244	210	132	104	34	22
SD (MPa)	4.6	0.4	0.6	6.1	10.3	15.4	1.7	1.3	6.0	0.0
f_u (MPa)	601	535	556	597	521	372	179	121	46	39
SD (MPa)	8.1	2.5	12.6	4.4	6.9	11.2	0.7	4.0	0.5	0.0

Table 2 shows the mean values of elastic modulus (E), yield stress (f_y), and ultimate strength (f_u) given in the temperature range of 20°C to 1000°C. The mechanical properties within this temperature range are relevant to fully describe the properties relevant during a welding operation. It can be seen how the elastic modulus, yield stress, and ultimate strength generally decrease as the temperature increases.

Welding Experiments

The following three subsections describe the welding experiments. The first subsection concerns the test weld specimens, while the second and third subsections concern the SAW process and HLAW process, respectively.

WELD SPECIMENS

The geometry of the welding application comprises a full penetration, one-sided butt weld joining two identical plates, each with dimensions of 480 × 240 × 10 mm. The plate edges have been prepared by water jet cutting, and the weld grooves have been prepared by milling. The weld grooves are different for the two welding methods and will thus be described in the following two subsections. Fig. 3 shows an isometric view of the test plate geometry and welding direction.

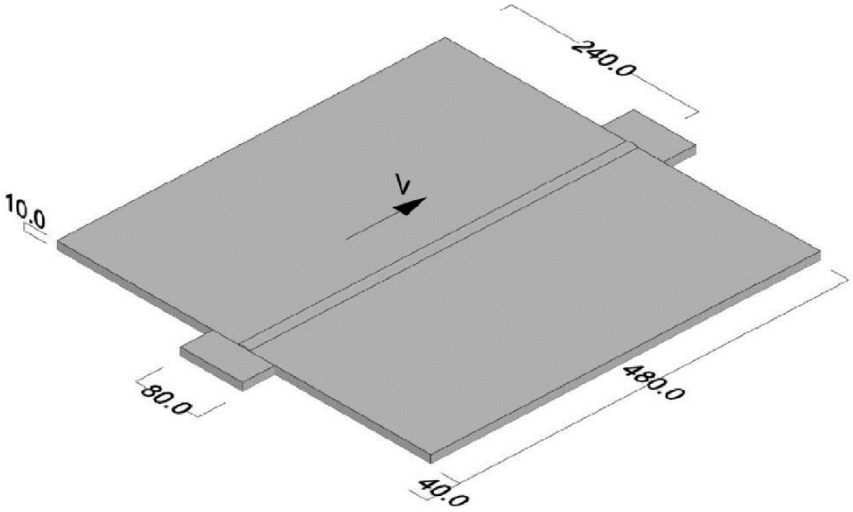

Figure 3: Isometric view of weld specimen geometry in mm.

The two main plates have been constrained (tack-welded) by a run-on and run-off plate of 80 × 40 × 10 mm at each end of the welded plate.

SAW EXPERIMENTS

The SAW butt-weld consists of two weld passes, a root pass and a cover pass, which have an interpass time of 940 seconds. The weld geometry comprises a bezel angle of 35°, nose height of 3.0 mm, and nose opening of 3.0 mm. An underlying bench supports the plates in the vertical downward direction.

Table 3: Welding procedure specifications for SAW.

Pass	AC/DC	Efficiency	Wire (mm)	Current (A)	Voltage (V)	Travel Speed (mm/min)	Heat Input (kJ/mm)
SAW 1	DC+	0.98	4	535	27.3	360	2.4
SAW 2	DC+	0.98	4	535	27.3	360	2.4

Table 4: Properties of filler wire and flux powder.

	C (%)	Si (%)	Mn (%)	P (%)	S (%)	Cu (%)	f_y (MPa)	f_u (MPa)	El. (%)	Impact Energy (J); T(°C)
OK Autrod 12.22/L	0.1	0.2	1.0	0.018	0.018	0.25	–	–	–	–
With OK flux 10.71/72	0.08	0.5	1.5	–	–	–	440	530	30	50; −40

Table 3 presents the welding procedure specification, and Table 4 presents the filler wire and flux powder properties. Figure 4 shows a cross-sectional macrograph of the SAW, and Figure 5 shows the welding test setup, including installed thermocouples.

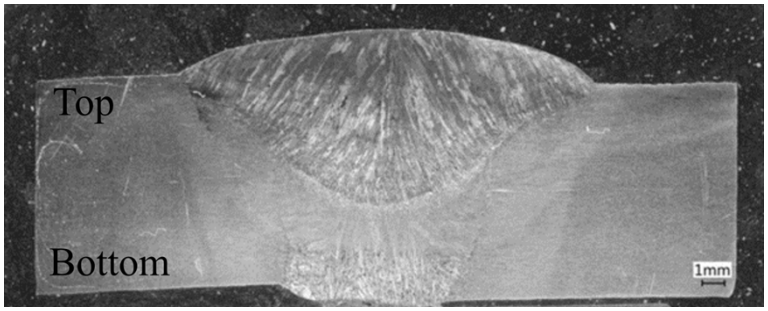

Figure 4: Cross sectional macrograph of SAW weld.

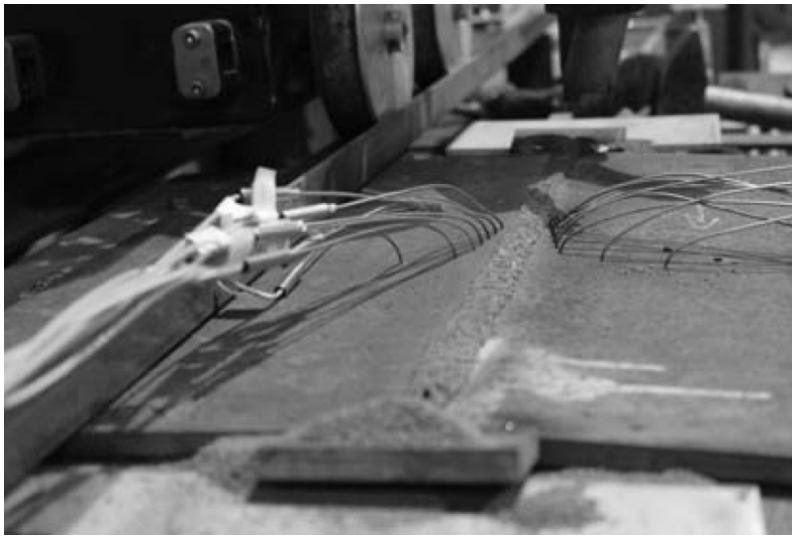

Figure 5: SAW welding test setup with thermocouples.

HLAW EXPERIMENTS

HLAW consists of two passes: first, a Metal Active Gas (MAG) weld pass from the bottom side of the plates, followed by a hybrid laser-arc pass from the top side. The MAG pass is performed in order to reduce the risk of laser beam penetration between the two plates. The HLAW equipment consists of a setup including a welding robot connected with MAG welding equipment and two 16-kW TruDisk lasers, which can be combined as a single laser equivalent to a 32-kW laser. The weld geometry comprises a bevel angle of 15°, nose height of 5.0 mm, and nose opening of 0.0 mm. The groove angle is only used for the MAG pass. Consequently, the HLAW pass is performed from the opposite side without any groove angle. An underlying bench supports the plates in the vertical downward direction. The mixture of gas used for the MAG pass and HLAW pass is 92% argon and 8% carbon dioxide.

Table 5: Welding procedure specifications for the root pass (MAG) and cover pass (HLAW).

Pass	Travel Speed (m/min)	Wire Diameter (mm)	Stick out (mm)	MAG Current (A)	MAG Voltage (V)	Laser (kW)	Weld Speed (mm/min)
1 (MAG)	9.5	1.2	25	310	33.5	–	650
2 (HLAW)	9.5	1.2	25	310	25	8	1000

Table 6: Chemical composition (in wt. pct.) and mechanical properties of the wire OK Autrod 12.51 and weld.

	C (%)	Si (%)	Mn (%)	P (%)	S (%)	f_y (MPa)	f_u (MPa)	A4−A5 (%)	Z	Impact Energy (J); T (°C)
Min	0.06	0.80	1.40	–	–	–	–	–	–	– –
Max	0.14	1.00	1.60	0.025	0.025	–	–	–	–	– –
As welded	0.10	0.72	1.11	0.013	0.012	470	560	26	68	130, 90, 70; 20, -20, -30

Table 5 provides the welding procedure specifications, and Table 6 lists the chemical composition and mechanical properties of the weld. Figure 6 shows a cross-sectional macrograph of the HLAW, and Figure 7 shows the welding test setup.

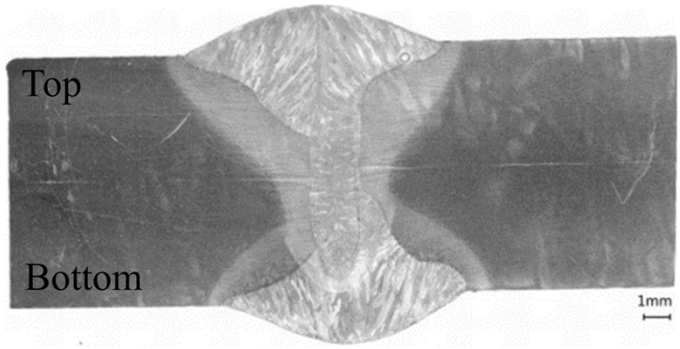

Figure 6: Cross sectional macrograph of HLAW weld.

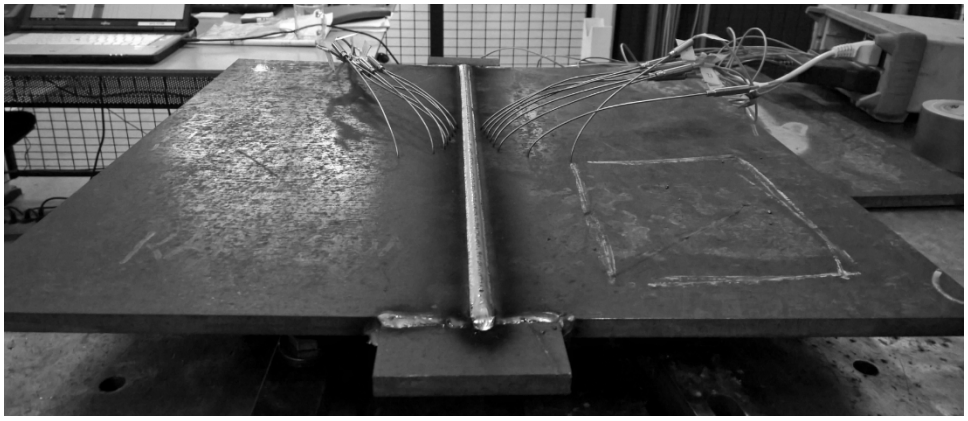

Figure 7: HLAW welding test setup with thermocouples.

TEMPERATURE DISTRIBUTION

Temperature measurements during welding are used to in-situ monitor the temperature evolution in the plates. The measurements guide the mapping of the residual stresses in the neutron diffraction experiments.

In the analysis of the thermal gradients from the welding procedure, it is desirable to have measurements as close as possible to the weld pool because of the buildup of residual stresses, which are highly influenced by the peak temperatures caused by the transient heat source. The distance between the thermocouples is therefore shortest close to the weld. The position of the thermocouples is in the middle of the plate, corresponding to 5 mm below the surface. The thermocouples are type "K" Mineral Insulated with a probe-diameter of 1.5 mm and length of 150 mm. A HP model 34970A data logger acquired the thermocouple data. The temperature measurements have an interval of 1 second. Figure 8 shows the thermocouple location, and Table 7 shows the distance to center of weld.

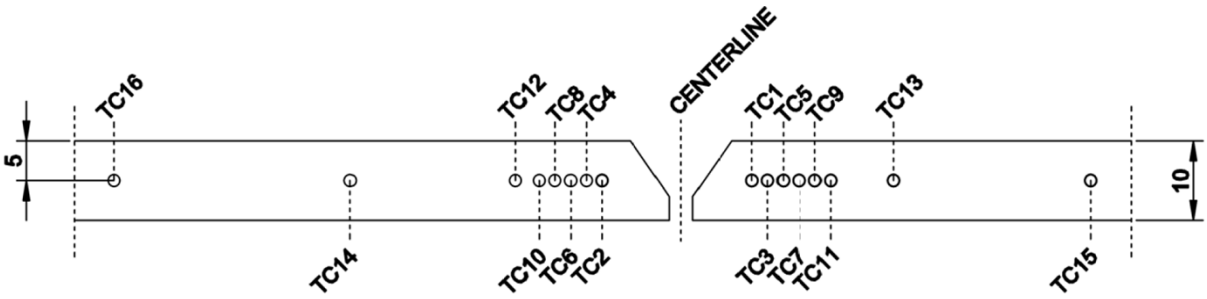

Figure 8: Location of temperature measurement points.

Tabel 7: Distance of thermocouples to center of weld.

I.D.	Dist. [mm]	I.D.	Dist. [mm]	I.D.	Dist. [mm]	I.D.	Dist. [mm]
TC 1	9	TC 5	13	TC 9	17	TC 13	27
TC 2	10	TC 6	14	TC 10	18	TC 14	42
TC 3	11	TC 7	15	TC 11	19	TC 15	52
TC 4	12	TC 8	16	TC 12	21	TC 16	72

SAW SPECIMENS

Figure 9 shows the measured transient temperatures for the SAW experiments. The temperature measurements for the first pass reached a maximum temperature of 641°C, and the second pass reached a maximum temperature of 692°C. The second pass was expected to have a higher

maximum temperature since it started at an initial temperature of 61°C compared with the room temperature for the first pass.

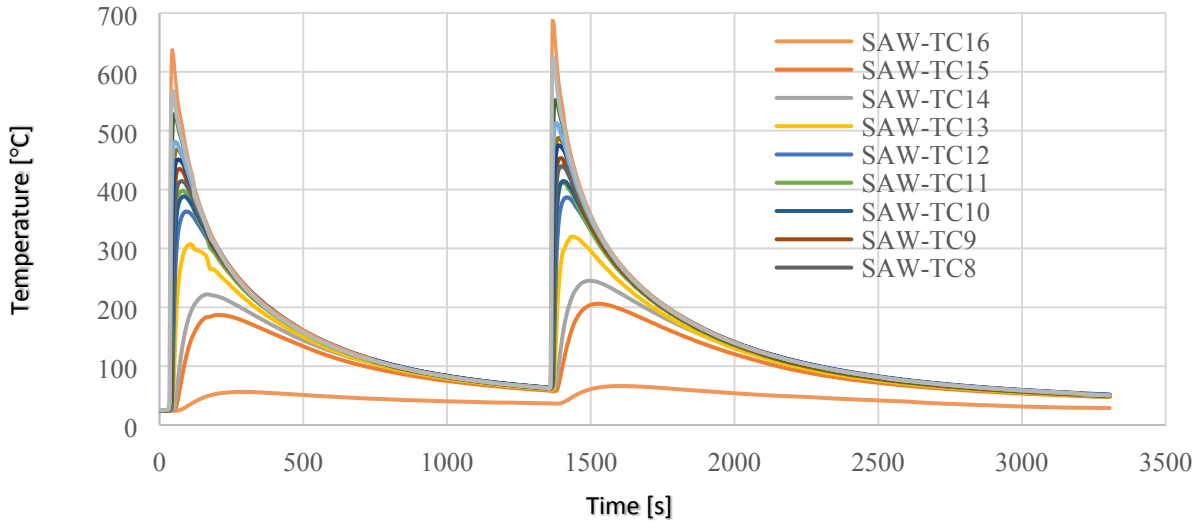

Figure 9: Measured transient temperatures for SAW experiments.

HLAW SPECIMENS

Figures 10 and 11 show the measured transient temperatures for the HLAW experiments. The MAG welding pass reached a maximum temperature of 314°C, and for HLAW, the maximum temperature was 414°C.

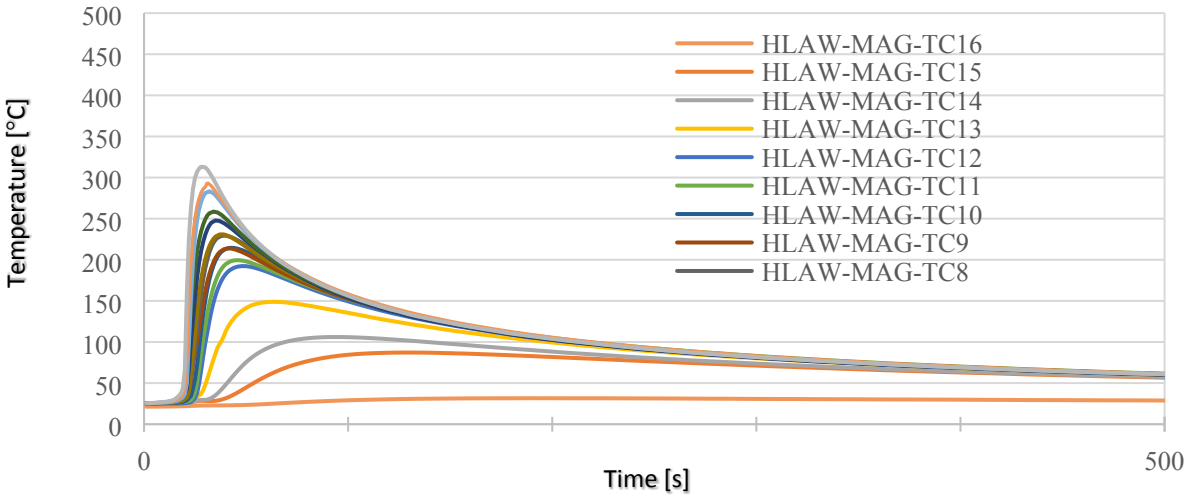

Figure 10: Measured transient temperatures for MAG pass in HLAW experiments.

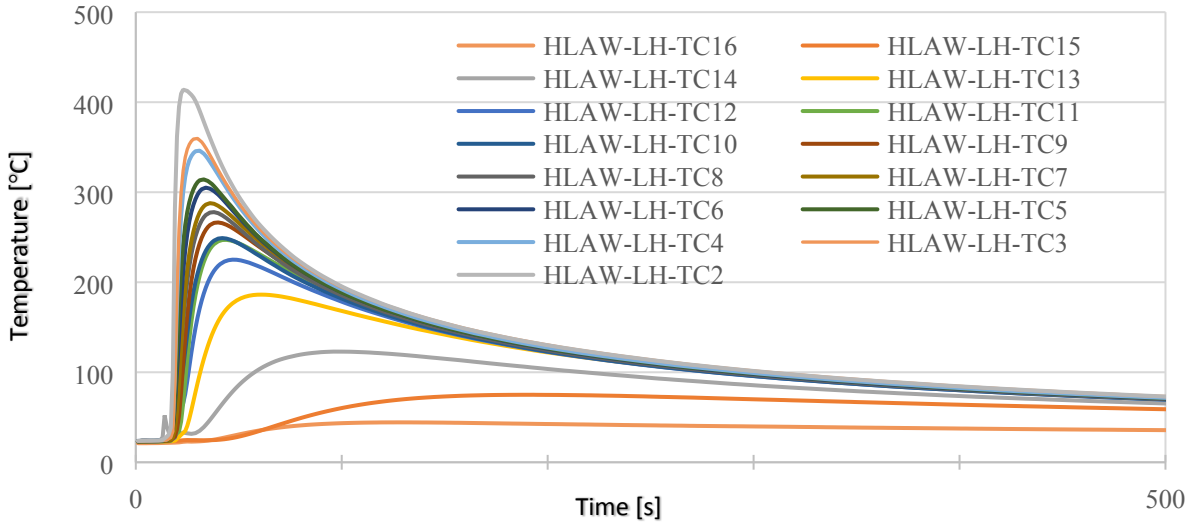

Figure 11: Measured transient temperatures for hybrid laser-arc pass in HLAW experiments.

Thus, the maximum measured transient temperature is higher in SAW than in HLAW.

RESIDUAL STRESS DISTRIBUTION

Neutron diffraction measurements were performed to map the residual stress distribution as a function of the distance away from the welds produced with the two different welding methods. The residual stress distribution is from the plate centerline cross section. The weld bead width is 10 mm for the SAW and 5 mm for HLAW. The lines of measurement points were performed at three different depths in the plates, and the d0-specimens are shown in Figure 12. The three different depths were 2 mm (top), 5 mm (center), and 8 mm (bottom) from the top side of the plate, respectively. Each line was repeated three times (run 1, run 2 and run 3), which means that nine lines in total were measured for each weld to map the strain distribution along three principal directions as a function of the distance away from the weld. This strain is then used for stress calculations.

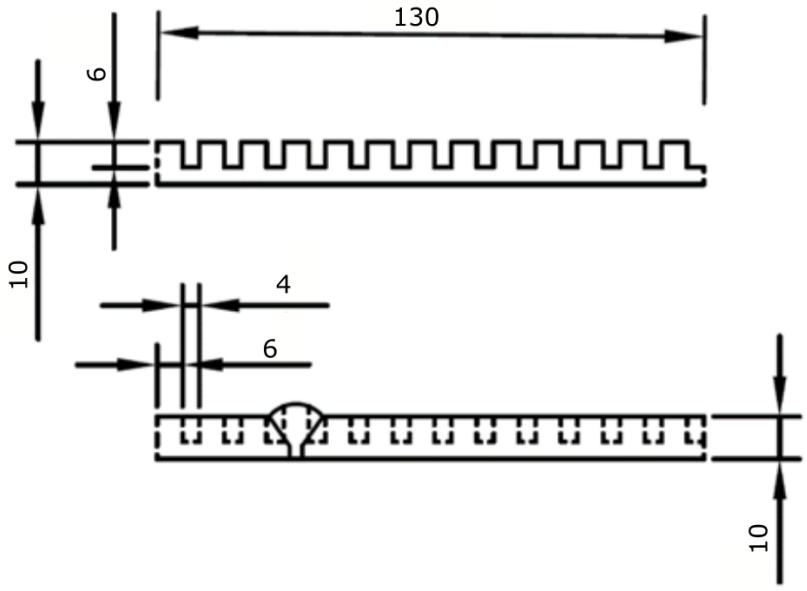

Figure 12: Geometry of d0-specimen in mm.

SAW SPECIMENS

Fig. 13 shows and compares the average calculated longitudinal residual stress distribution at all three depths for the SAW plate.

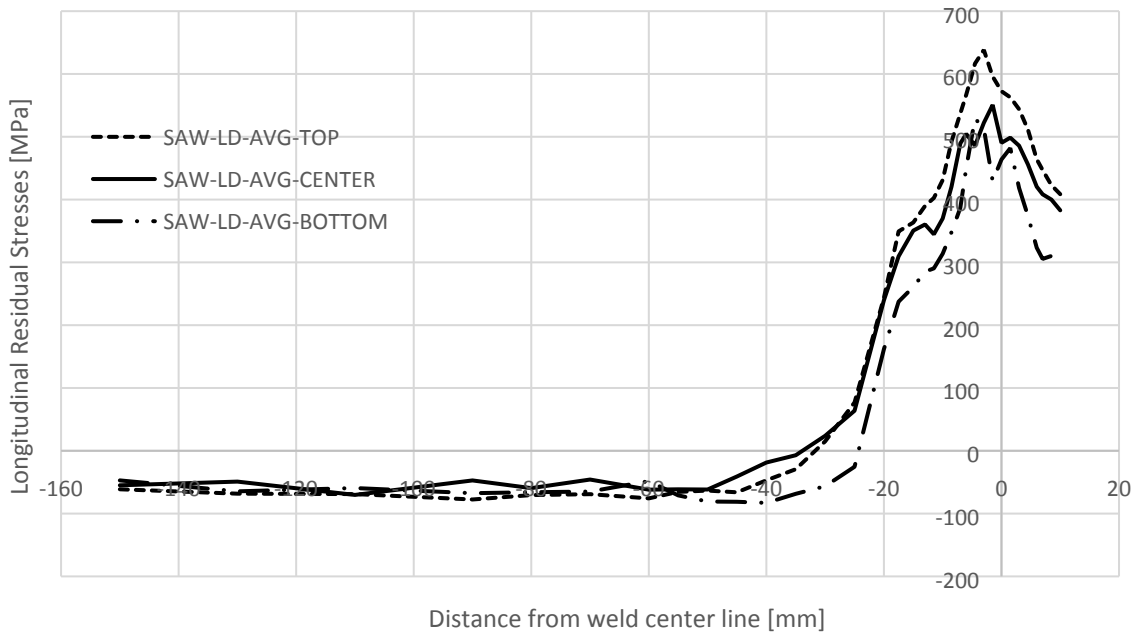

Figure 13: Longitudinal residual stresses for different plate depths for the SAW welding.

From Figure 13, it is seen that the average longitudinal residual stresses from all three runs are in tension close to the weld and in compression farther away from the weld. The tensional stresses are highest at the top of the plate. The maximum average absolute tensional longitudinal residual stresses are 638 MPa at the top of the plate, 551 MPa at the center of the plate, and 529 MPa at the bottom of the plate.

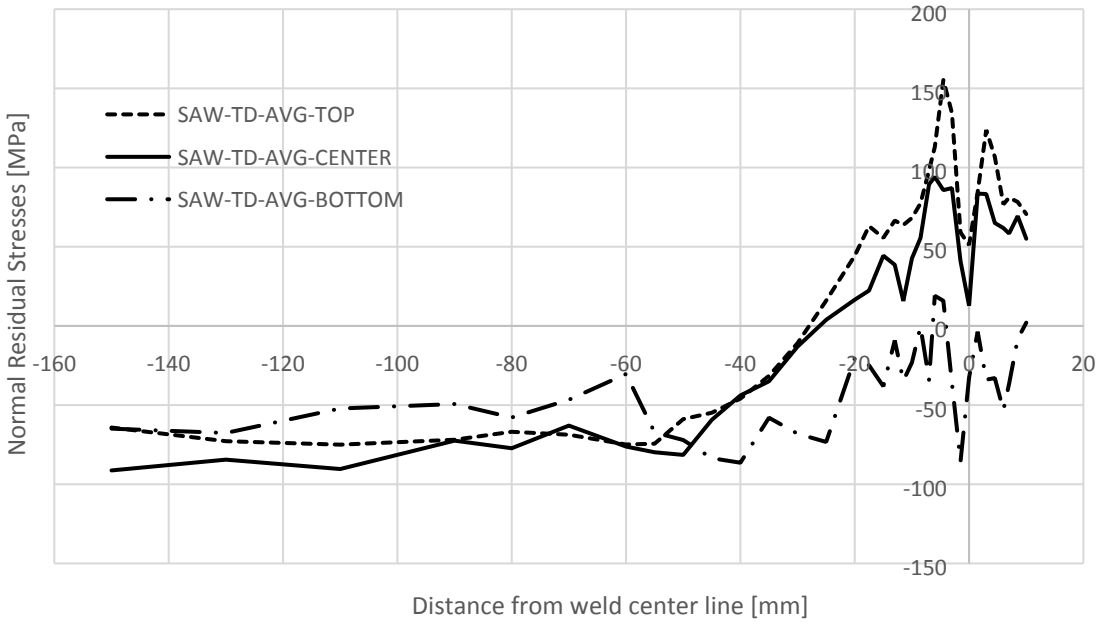

Figure 14: Transverse residual stresses at different plate depths for the SAW welding.

From Figure 14, it is seen that the average transverse residual stresses are in tension close to the weld and go to compression farther away from the weld. The tensional stresses are highest at the top of the plate. The maximum average absolute tensional transverse residual stresses are 168 MPa at the top of the plate, 136 MPa at the center of the plate, and −55 MPa at the bottom of the plate.

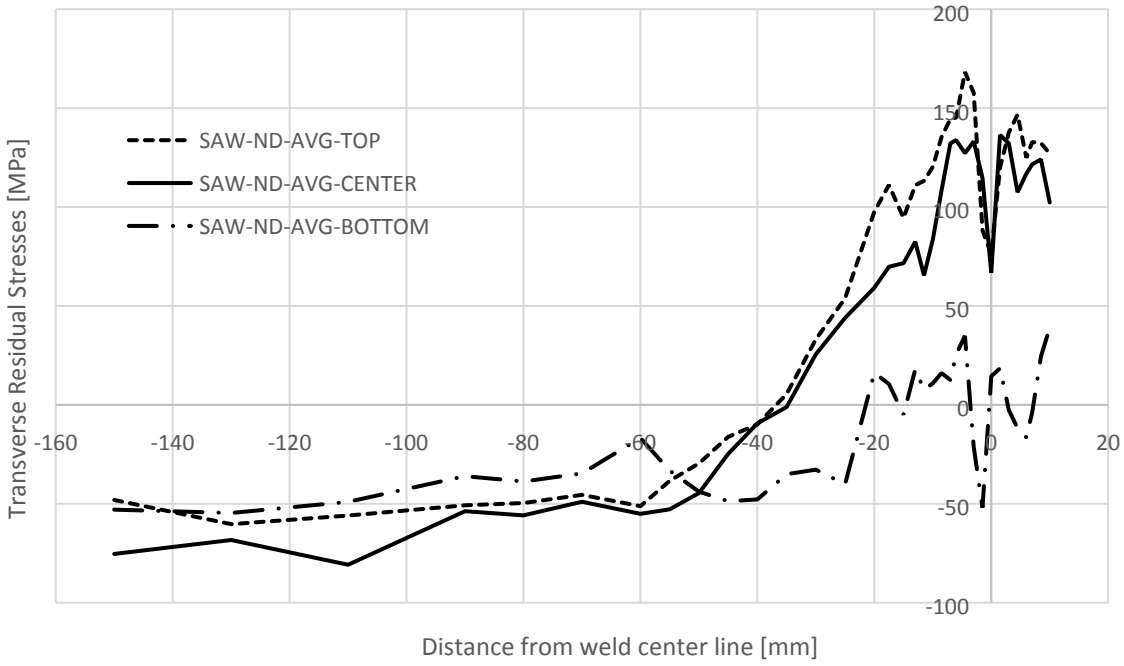

Figure 15: Normal residual stresses at different plate thicknesses for the SAW welding.

From Figure 15, it is seen that the average normal residual stresses are in tension close to the weld and go to compression farther away from the weld. The normal stresses are highest at the top of the plate. The maximum average absolute tensional transverse residual stresses are 155 MPa at the top of the plate, 94 MPa at the center of the plate, and −86 MPa at the bottom of the plate.

Considering the maximum measured residual stresses in the plate (at the top), we have approximately a longitudinal stress of $\sigma_{LD} = 638$ MPa, transverse stress of $\sigma_{TD} = 168$ MPa, and normal stress of $\sigma_{ND} = 155$ MPa. Assuming that these measured stresses are principal stresses, the von Mises stress criterion for yielding can be written as follows:

$$2\sigma_y^2 = (\sigma_{LD} - \sigma_{TD})^2 + (\sigma_{TD} - \sigma_{ND})^2 + (\sigma_{ND} - \sigma_{LD})^2$$

Inserting the given measured values, we obtain:

$$2\sigma_y^2 = (638-168)^2 + (168-155)^2 + (155-638)^2 \Leftrightarrow \sigma_y = 477 \text{ MPa}$$

which is in line with the material properties for the welding medium material according to Table 4, where a yield stress of 440 MPa and ultimate strength of 560MPa are found.

HLAW SPECIMENS

Fig. 16 shows and compares the longitudinal residual stress distribution at all three depths for HLAW.

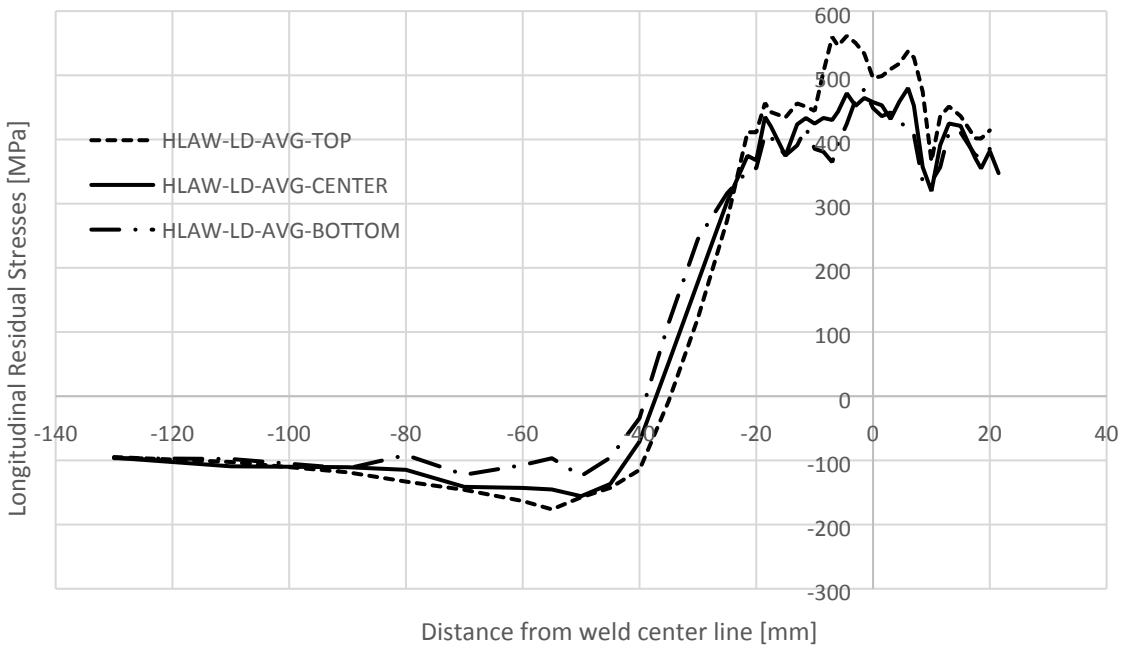

Figure 16: Longitudinal residual stresses at different plate depths for the HLAW welding.

From Figure 16, it is seen that for HLAW, the average longitudinal residual stresses are in tension close to the weld and go to compression farther away from the weld. The longitudinal stresses are highest at the top of the plate. The maximum average absolute tensional longitudinal residual stresses are 561 MPa at the top of the plate, 480 MPa at the center of the plate, and 478 MPa at the bottom of the plate.

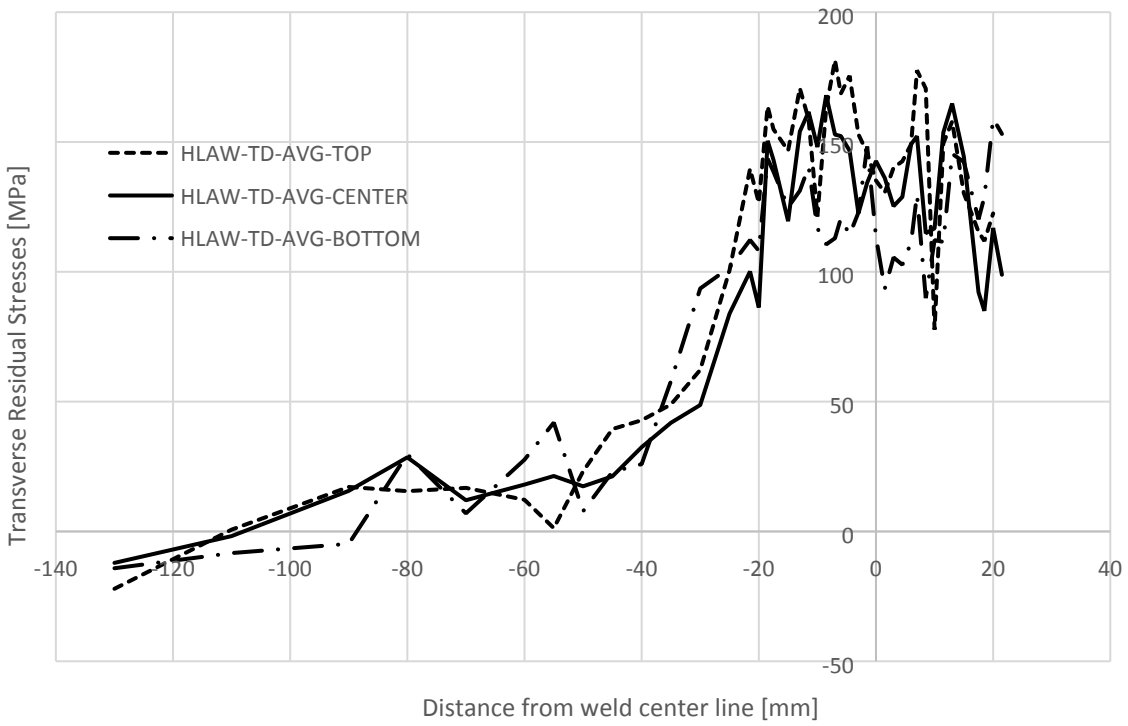

Figure 17: Transverse residual stresses at different plate depths for the HLAW welding.

From Figure 17, it is seen that the average transverse residual stresses are in tension close to the weld and go to compression farther away from the weld. The tensional stresses are highest at the top of the plate. The maximum average absolute tensional transverse residual stresses are 182 MPa at the top of the plate, 168 MPa at the center of the plate, and 159 MPa at the bottom of the plate.

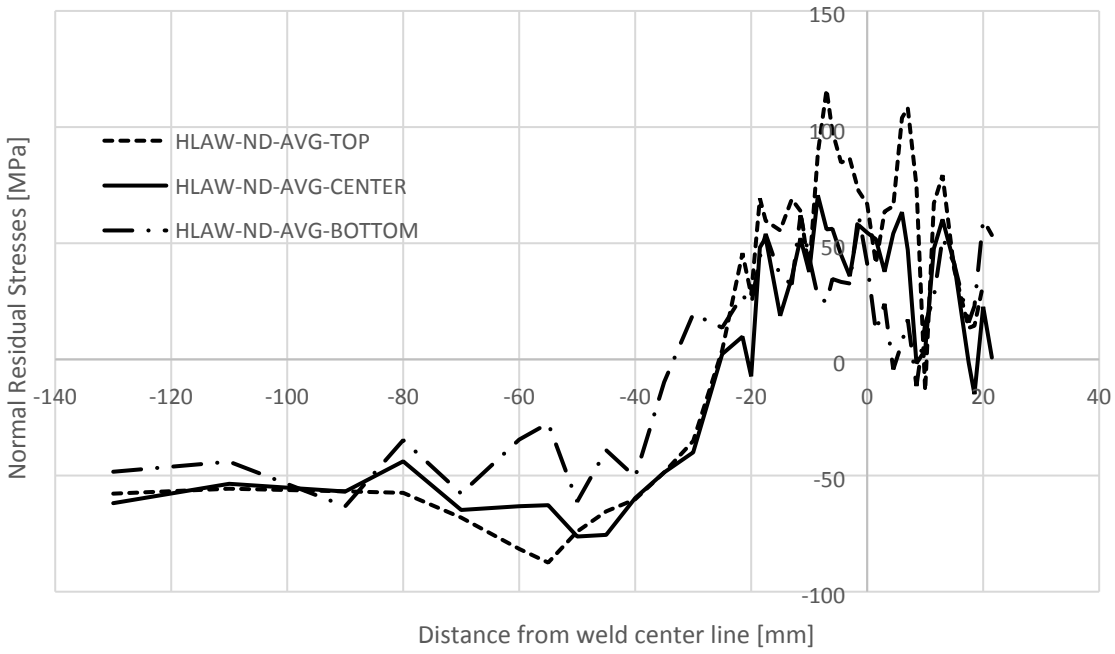

Figure 18: Normal residual stresses at different plate depths for the HLAW welding.

From Figure 18, it is seen that the average normal residual stresses are in tension close to the weld and go to compression farther away from the weld. The normal stresses are highest at the top of the plate. The maximum average absolute tensional transverse residual stresses are 116 MPa at the top of the plate, 71 MPa at the center of the plate, and 62 MPa at the bottom of the plate.

The most critical stresses related to fatigue are the tensional stresses. From Figures 16-18, it is seen that the tensional stresses are largest at the top of the plates. This makes sense, as the first welding pass, which is at the bottom of the plate, is annealed by the following second pass and thus has lower residual stresses.

Considering the maximum measured residual stresses in the plates (at the top) for HLAW, we have approximately a longitudinal stress of $\sigma_{LD} = 561$ MPa, a transverse stress of $\sigma_{TD} = 182$

MPa, and a normal stress of $\sigma_{ND} = 116$ MPa. Assuming that these stresses follow the principal directions, we can write the von Mises stress criterion as follows:

$$2\sigma_y^2 = (\sigma_{LD} - \sigma_{TD})^2 + (\sigma_{TD} - \sigma_{ND})^2 + (\sigma_{ND} - \sigma_{LD})^2$$

Inserting the given values, we obtain:

$$2\sigma_y^2 = (561 - 182)^2 + (182 - 116)^2 + (116 - 561)^2 \Leftrightarrow \sigma_y = 416 \text{ MPa}$$

which is in line with the material properties for the welding consumable and base material, according to Tables 2 and 6.

SAW COMPARED WITH HLAW

In this section, the average maximum residual stresses for the SAW and HLAW methods will be compared.

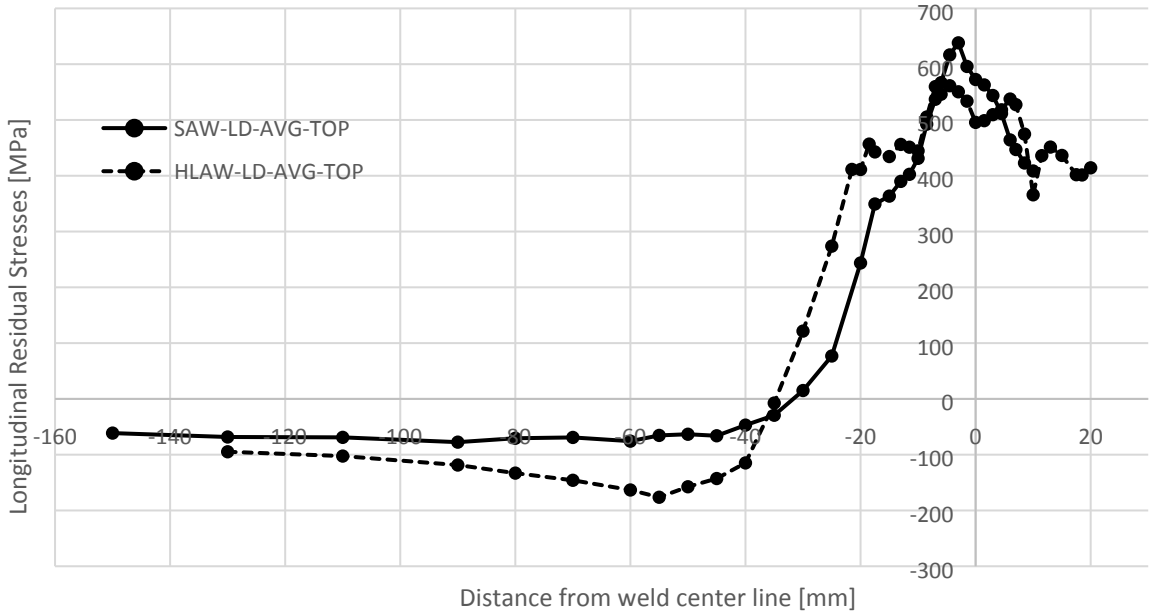

Figure 19: Comparison of longitudinal residual stresses for the SAW and HLAW.

From Fig. 19, it is seen that the maximum SAW stress is 638 MPa compared with 561 MPa for HLAW. Furthermore, the minimum stress for the SAW is −83 MPa compared with −176 MPa for HLAW.

This means that the longitudinal tensional stresses are higher for SAW than HLAW; however, the longitudinal compressive stresses are higher for HLAW than SAW. This makes sense because the stresses must balance. If the tensile stress is increased, then it follows to reason that the compressive stresses must also increase for equilibrium to be maintained. Furthermore, it is seen that the longitudinal stress distribution is wider for HLAW than SAW. This observation is opposite to what is reported in Andreassen et al. [13].

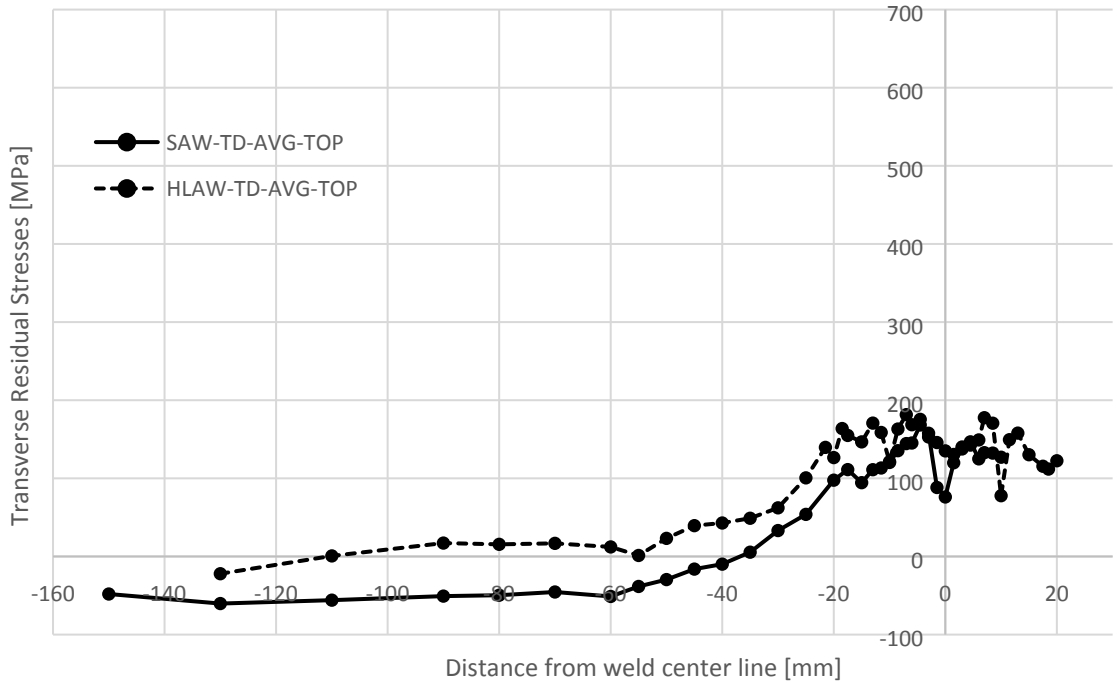

Figure 20: Comparison of transverse residual stresses for the SAW and HLAW.

From Fig. 20, it is seen that the maximum SAW transverse stress is 168 MPa compared with 182 MPa for HLAW. Furthermore, the minimum stress for SAW is −81 MPa compared with −22 MPa for HLAW.

This means that the transverse tensional stresses are slightly higher for HLAW than SAW, and the transverse compressive stresses are higher for SAW than HLAW.

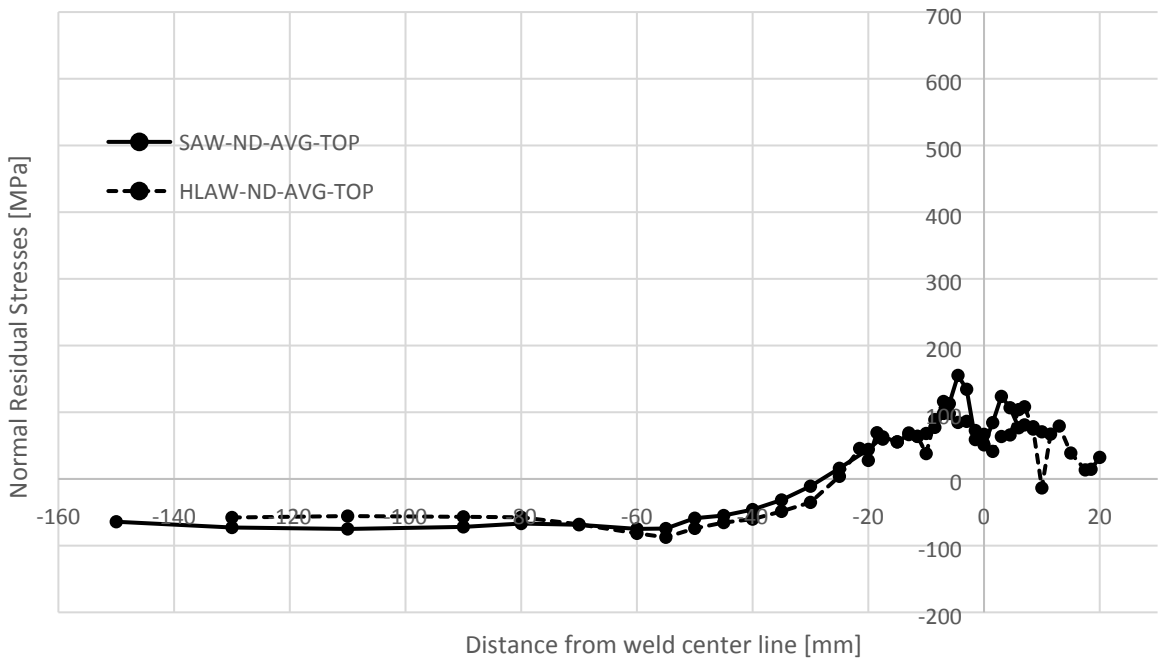

Figure 21: Comparison of normal residual stresses for the SAW and HLAW.

From Fig. 21, it is seen that the maximum SAW stress is 155 MPa compared with 116 MPa for HLAW. In addition, the minimum stress for SAW is –91 MPa compared with –87 MPa for HLAW.

Thus, the normal tensional stresses are higher for SAW than HLAW, and the normal compressive stresses are higher for SAW.

REPEATABILITY OF NEUTRON DIFFRACTION MEASUREMENTS

The neutron diffraction measurements of the residual stresses at the top were repeated three times. In Fig. 22 the results are presented.

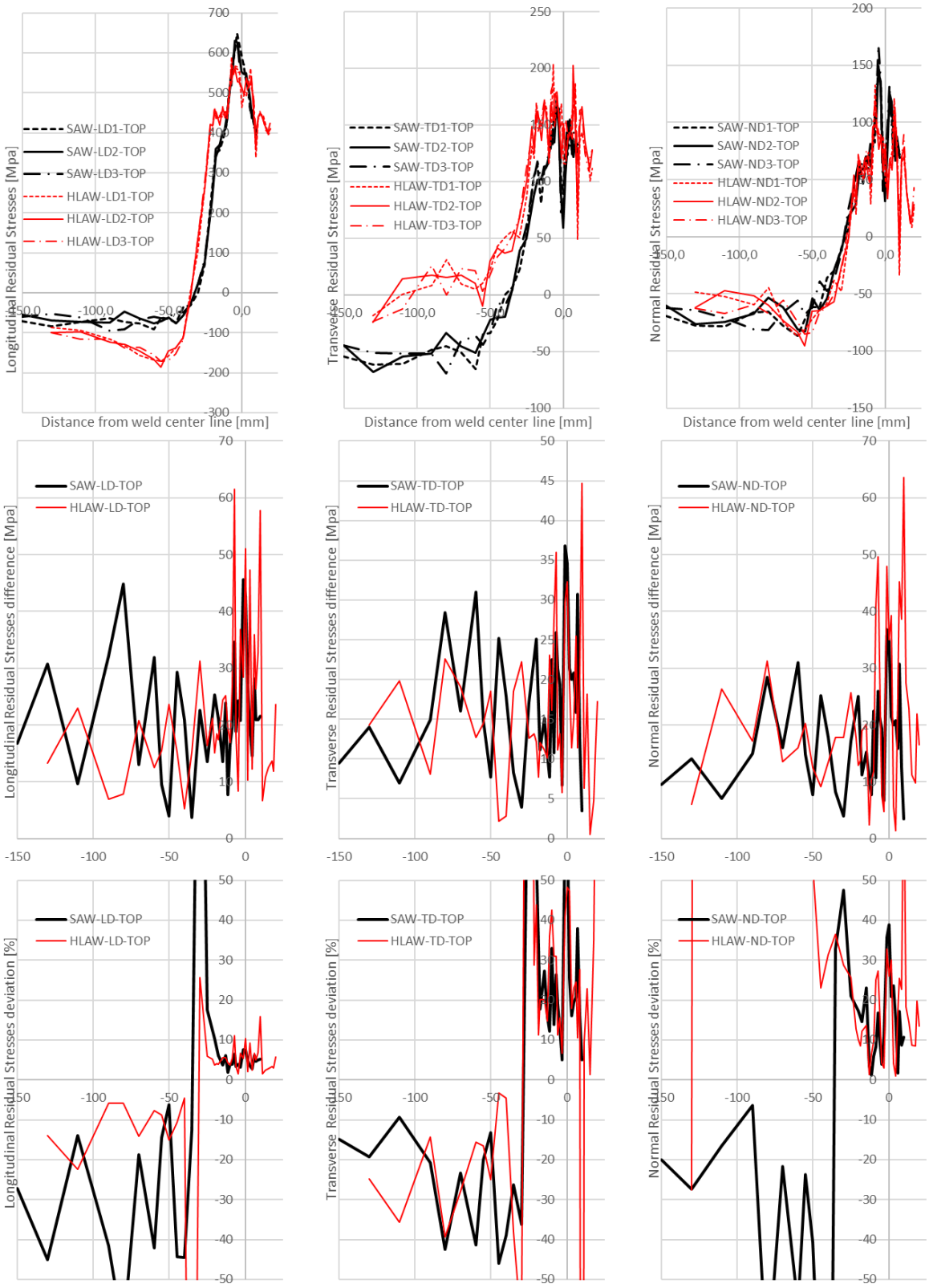

Figure 22: Repeatability of the neutron diffraction measurements.

Each column represents (from left to right) the different stress directions: Longitudinal Direction (LD), Transverse Direction (TD), and Normal Direction (ND). The first row of plots shows the stresses measured in the two specimens, while the second provides the maximum difference between the three measurements. The last row provides a relative deviation in percent found by dividing the maximum difference with the average measured residual stress and recalculated into percent. The vertical axis of the deviation has been cut off at 50% because of unrealistic relative deviation when the average of the residual is close to zero.

From Figure 22, it is seen that the shape of the residual stress state could be reproduced. It is also worth noting that, as expected, the welding technique does not seem to affect the reproducibility. However, it is worth noting that the deviation for the transverse and normal stress seems to be rather high. For the longitudinal stress, a deviation of 5–10 % in the weld area is observed, and, in general, a scatter of approximately 15–20 MPa is seen independent of the stress level.

Conclusions

Welding residual stresses have been mapped and analyzed in two different butt welds made by SAW and HLAW of 10-mm-thick steel plates. Experimental temperature profile measurements and neutron diffraction measurements have been used to map the residual stress distributions in three different depths of the plates.

In both plates, the longitudinal, transverse, and normal stresses are highest at the top side of the plate. The maximum stresses are the tensional stresses in the longitudinal direction. HLAW has a wider distribution of the longitudinal residual stresses than SAW; however, HLAW has a lower maximum value of longitudinal tensile stresses than SAW. The longitudinal compressive stresses are higher for HLAW than SAW. For both welding methods, the

maximum longitudinal residual stresses are above the uniaxial yield strength of the steel material.

The transverse tensional stresses are slightly higher for HLAW than for SAW; however, the normal tensional stresses are higher for SAW than HLAW.

In general, the repeatability for the neutron diffraction stress measurements shows a difference of up to 20 MPa, irrespective of stress direction. This is consistent with what the neutron beam instrument staff expect; a change of ±50 με is the quoted maximum achievable instrumental strain resolution, and with material effects, this is increased to roughly ±100 με.

ACKNOWLEDGMENTS

The authors are grateful to Lindoe Welding Technology (Munkebo, Denmark) for the support provided production of the HLAW welded specimens. Furthermore, the authors are grateful to DOE Office of Science, BES, for awarding neutron beam time at the High Flux Isotope Reactor (HFIR) at Oak Ridge National Laboratory (Oak Ridge, TN, United States).

References

[1] Jacob, A., Oliveira, J., Mehmanparast, A., Hosseinzadeh, F., Kelleher, J., Berto, F. (2018). Residual stress measurements in offshore wind monopile weldments using neutron diffraction technique and contour method. Theoretical and Applied Fracture Mechanics, Volume 96, pp. 418-427.

[2] Colegrove, P., et al. (2009). The welding process impact on residual stress and distortion. Science and Technology of Welding and Joining, Vol 14 (8), pp. 717-725.

[3] Mehmanparast, A., el al.(2016). Welding sequence effects on residual stress distribution in

offshore wind monopile structures. Frattura Ed Integrita Strutturale. Vol 10 (35), pp. 125-131.

[4] Pedersen, M.M., Andersen J.G., Olafsson, O.M. (2012). Investigation of the thickness effect for butt welded joints. IIW, WG1-154-12.

[5] Anis M. (2011). Effect of Plate Thickness and Weld Position on Distortion and Residual Stress of Welded Structural Steel. Materials Science Forum, Vol. 689, pp. 296-301.

[6] Eurocode 3: "Design of steel structures – Part 1–9: Fatigue". Danish Standard, 2005.

[7] Det Norske Veritas, DNV-OS-J101, Design of Offshore Wind Turbine Structures. DNV, 2010.

[8] Krebs J., et al: Influence of Welding Residual Stresses on Fatigue Design of Welded Joints and Components: IIW Doc. IIW-1805-07: 2007.

[9] Andreassen, Michael Joachim; Yu, Zhenzhen; Liu, Stephen, Nielsen, Jens Henrik. The Influence of Plate Thickness on the Welding Residual Stresses from Submerged Arc Welding in Offshore Steel Structures. EUROSTEEL 2017, Copenhagen, Denmark. 2017.

[10] DS/EN 10025-4-2004, Hot rolled products of structural steels – Part 4: Technical delivery conditions for thermomechanical rolled weldable fine grain structural steels, 2004.

[11] DS-EN ISO 6892-1-2013 – Metallic material – Tensile testing Part 1: Method of test at room temperature.

[12] DS-EN ISO 6892-2-2013 – Metallic material – Tensile testing Part 2: Method of test at elevated temperature.

[13] Andreassen, Michael Joachim; Yu, Zhenzhen; Liu, Stephen, Martha Patricia Guerrero-Mata. Comparison of Welding Residual Stresses of Hybrid Laser-Arc Welding and Submerged Arc Welding in Offshore Steel Structures. 10th International Conference on Trends in Welding Research. Tokyo. Japan. 2016.

List of Figure Captions

FIG. 18 Normal residual stresses at different plate thicknesses for the HLAW welding.

FIG. 19 Comparison of longitudinal residual stresses in the SAW and HLAW welding's.

FIG. 20 Comparison of transverse residual stresses in the SAW and HLAW welding's.

FIG. 21 Comparison of normal residual stresses in the SAW and HLAW welding's.

FIG. 22 Repeatability of the neutron diffraction measurements.